Low mutation burden and frequent loss of *CDKN2A/B* and *SMARCA2*, but not PRC2, define pre-malignant neurofibromatosis type 1-associated atypical neurofibromas

Alexander Pemov[1], Nancy F. Hansen[2], Sivasish Sindiri[3], Rajesh Patidar[4,3], Christine S. Higham[5,6], Eva Dombi[6], Markku M. Miettinen[7], Patricia Fetsch[7], Hilde Brems[8], Settara Chandrasekharappa[2], Kristine Jones[9], Bin Zhu[9], Jun S. Wei[3], NISC Comparative Sequencing Program[10], NCI DCEG Cancer Genomics Research Laboratory[9], James C. Mullikin[2,10], Margaret R. Wallace[11], Javed Khan[3], Eric Legius[8], Brigitte C. Widemann[6] and Douglas R. Stewart[1]

[1]Clinical Genetics Branch, Division of Cancer Epidemiology and Genetics, National Cancer Institute, NIH, Rockville, MD, USA

[2]Cancer Genetics and Comparative Genomics Branch, National Human Genome Research Institute, NIH, Rockville, MD, USA

[3]Genetics Branch, Center for Cancer Research, National Cancer Institute, NIH, Bethesda, MD, USA

[4]Molecular Characterization & Clinical Assay Development Laboratory, Frederick National Laboratory for Cancer Research, Leidos Biomedical Research, Inc., Frederick, MD, USA

[5]Children's National Medical Center, Washington, DC, USA

[6]Pediatric Oncology Branch, Center for Cancer Research, National Cancer Institute, NIH, Bethesda, MD, USA

[7]Laboratory of Pathology, National Cancer Institute, NIH, Bethesda, MD, USA

[8]Department of Human Genetics, Catholic University Leuven, Leuven, Belgium

[9]Cancer Genomics Research Laboratory, Division of Cancer Epidemiology and Genetics, National Cancer Institute, NIH, Rockville, MD, USA

[10]NIH Intramural Sequencing Center, National Human Genome Research Institute, NIH, Rockville, MD, USA

[11]Dept of Molecular Genetics and Microbiology, UF Genetics Institute, UF Health Cancer Center, University of Florida, Gainesville, FL, USA

Running title: Loss of *CDKN2A/B* and *SMARCA2*, but not PRC2, in ANF

Corresponding author: Douglas R. Stewart (drstewart@mail.nih.gov; Tel: 240-276-7238; Fax: 240-276-7836; 9609 Medical Center Drive Rm 6E450, Bethesda, MD, 20892)

Funding: This work was supported by the Intramural Research Program of the Division of Cancer Epidemiology and Genetics and the Center for Cancer Research of the National Cancer Institute, Bethesda, MD.

Conflict of Interest: The authors declare no conflict of interest.

Authorship: AP – performed experiments, analyzed data, wrote and prepared manuscript for publication, submitted manuscript for publication; NFH – analyzed high-throughput data, wrote portion of the manuscript; SS - analyzed high-throughput data, wrote portion of the manuscript; RP - analyzed high-throughput data, wrote portion of the manuscript; CSH – collected and analyzed clinical data, wrote portion of the manuscript; ED - analyzed clinical data, wrote portion of the manuscript; MMM – performed pathology analysis of tumors; PF – prepared tumor tissues for pathology analysis; HB – collected surgical material, isolated DNA from blood and tumors, collected and analyzed clinical data; SC – performed SNP-microarray experiments, wrote portion of the manuscript; KJ – performed high-throughput experiments, wrote portion of the manuscript; BZ - analyzed high-throughput data, wrote portion of the manuscript; JSW - wrote portion of the manuscript; JCM – contributed to experimental design and its implementation; MRW - contributed to experimental design and its implementation; JK - contributed to experimental design, its implementation and interpretation of the data; EL – provided

biospecimens, contributed to experimental design and interpretation of the data; BCW - provided biospecimens, contributed to experimental design and its implementation, wrote portion of the manuscript; DRS - contributed to experimental design, its implementation and interpretation of the data, wrote portion of the manuscript.

Word count: 5,950

Total number of tables and figures: 6

Abstract

Background. Neurofibromatosis type 1 (NF1) is a tumor-predisposition disorder caused by germline mutations in *NF1*. NF1 patients have an 8-16% lifetime risk of developing a malignant peripheral nerve sheath tumor (MPNST), a highly-aggressive soft-tissue sarcoma, often arising from pre-existing benign plexiform neurofibromas (PN) and atypical neurofibromas (ANF). ANF are distinct from both PN and MPNST, representing an intermediate step in malignant transformation. **Methods.** In the first comprehensive genomic analysis of ANF originating from multiple patients, we performed tumor/normal whole-exome sequencing (WES) of 16 ANFs. In addition, we conducted WES of three MPNSTs, copy-number meta-analysis of 26 ANFs and 28 MPNSTs, and whole transcriptome sequencing analysis of five ANFs and five MPNSTs. **Results.** We identified a low number of mutations (median 1, range 0-5) in the exomes of ANFs (only *NF1* somatic mutations were recurrent), and frequent deletions of *CDKN2A/B* (69%) and *SMARCA2* (42%). We determined that polycomb repressor complex 2 (PRC2) genes *EED* or *SUZ12* were frequently mutated, deleted or downregulated in MPNSTs but not in ANFs. Our pilot gene expression study revealed upregulated *NRAS*, *MDM2*, *CCND1/2/3* and *CDK4/6* in ANFs and MPNSTs, and overexpression of *EZH2* in MPNSTs only. **Conclusions.** The PN-ANF transition is primarily driven by the deletion of *CDKN2A/B.* Further progression from ANF to MPNST likely involves broad chromosomal rearrangements and frequent inactivation of the PRC2 genes, loss of the DNA repair genes, and copy-number increase of signal transduction, cell cycle and pluripotency self-renewal genes.

Key words: Neurofibromatosis type 1; plexiform neurofibromas; atypical neurofibromas; malignant peripheral nerve sheath tumor; benign-to-malignant transformation

Key points: ANF are relatively chromosomally-stable tumors with low somatic mutation burden; frequent inactivation of *NF1*, *CDKN2A/B*, *SMARCA2* genetically defines ANF; unlike MPNST, we detect no recurrent PRC2 gene inactivation in ANF

Importance of the Study

NF1-associated ANF are rare pre-malignant lesions with a high risk of transformation to MPNST, a soft-tissue sarcoma with poor prognosis. Early detection and treatment of ANF may prevent MPNST, for which surgery remains the only therapeutic option. At present, the genetics of ANF development and transformation to MPNST are not fully understood. Here we present the first multi-sample/multi-patient comprehensive genomic study of ANF. We show that somatic mutation burden and genomic instability in ANF is relatively low, with only *NF1*, *CDKN2A/B* and, to a lesser extent, *SMARCA2* mutated in the tumors. *SUZ12*, *EED* or *TP53*, which are frequently inactivated in MPNST, are intact in ANF. We conclude that in ANF, loss of *CDKN2A/B* is the main genetic event that in addition to *NF1* inactivation leads to pre-malignancy. The transition to MPNST coincides with a dramatic rise in genomic instability, inactivation of PRC2 and copy-number gains of cell-cycle and pluripotency genes.

Introduction

Neurofibromatosis type 1 (NF1) is a common (~1/2000 – 1/3500 worldwide [1]) autosomal dominant, archetypal tumor-predisposition disorder secondary to mutations in the tumor suppressor *NF1*. Phenotypically, NF1 is associated with neurocutaneous abnormalities, including a variety of benign and malignant tumors[2]. Life expectancy is reduced by 8-15 years in both men and women, primarily due to malignancy and cardiovascular disease[3,4]. A significant proportion of the excess mortality in NF1 is attributable to malignant peripheral nerve sheath tumors (MPNST), an aggressive soft-tissue sarcoma with limited therapeutic options[4]. The relative risk of MPNST in NF1 is enormously increased (~2000-fold), with a lifetime risk of 8-16%[4,5].

MPNSTs typically arise from a pre-existing plexiform neurofibroma (PN), a histologically benign congenital neurofibroma affecting up to 50% of people with NF1[6] and readily identified on whole-body MRI (WBMRI)[7]. More widespread use of WBMRI has prompted the identification of "distinct nodular lesions" (DNL), frequently within PNs. These lesions are >3 cm in longest diameter, well-demarcated, distinct from surrounding tissue and lack the "central dot" sign of PN. Distinct nodular lesions appear after early childhood and typically grow faster than the surrounding or adjacent PN and may be precursors of an MPNST[8]. Some DNL are biopsy-proven atypical neurofibromas (ANF)[9]. ANF are pathologically defined lesions that have increased variable cellularity, cytological atypia, and more pronounced fascicular growth patterns, but lack the widespread atypia and fascicular growth mitotic activity and necrosis seen in MPNST. In one study, 15/16 ANFs harbored a deletion of chromosome 9p21.3, a region that includes cell-cycle regulators *CDKN2A/B* [10], both frequently deleted somatically in MPNSTs[11-14].

The ANF is hypothesized to be a pre-malignant lesion, with *CDKN2A/B* deletion the first step in the progression to MPNST. WES and copy-number analysis of PNs showed remarkably low somatic mutation rates, stable chromosomal architecture, intact *CDKN2A/B* and revealed the primacy of *NF1* inactivation in its pathogenesis[15]. WES of NF1-associated MPNST shows that biallelic loss of *NF1* and

mutation in PRC2 genes are essential to its pathogenesis[16-18]. It remains unclear what other genes and pathways play a role in PN transformation into a pre-malignant state. Resection of ANF may prevent MPNST[9]; therefore, identification of genetic biomarkers for ANF is important for the disease management. A better understanding of the PN-to-MPNST transformation is key recommendation from a recent international consensus meeting on research priorities in MPNST[19,20]. To investigate this, we characterized ANFs and a small set of MPNSTs using WES, whole transcriptome sequencing and copy-number determination.

Materials and Methods

Sample collection and clinical information. Clinical information and tumor samples with matching normal DNA were collected at the US National Cancer Institute (Bethesda, MD, USA), the University of Leuven (Leuven, Belgium) and the University of Florida (Gainesville, FL, USA). The diagnosis of all ANF cases was confirmed by one pathologist at NCI and one pathologist at the University of Leuven. All protocols were approved by the appropriate investigational review board and subjects and/or their parents or guardians provided written, informed consent. Detailed description of the materials and methods used in this study can be found in Supplementary File 1.

Whole-exome sequencing of matching pairs of tumor and normal DNA. Capture of the exome and library preparation was done using SeqCap EZ Exome plus UTR Library kit (Roche, #06740308001). Sequencing was done according to the manufacturer's instructions. Among sequenced exomes, the average breadth of coverage was 89% of targeted bases (range 88%-91%), and the average depth of coverage was 59X (range 44X-82X) for both tumor and normal samples.

Whole-exome sequencing analysis. Sequencing reads were aligned to NCBI Build GRCh37 (hg19) using Novoalign v.2.08.02 (for ANF1 through ANF7) and v.3.02.07 (for ANF8 through ANF15). Point mutations and small indels were called for all tumor-normal pairs with Mutect (v.1.1.4)[21], SomaticSniper (v.1.0.5)[22] and Shimmer (v.0.1.1)[23]. Mutect and Shimmer used default parameters; filtering of SomaticSniper variants

was as per program authors. MPNST samples were analyzed in the same manner, except that an additional somatic caller, Strelka v.1.0.14[24], was added to the pipeline. Coding variants identified as somatic mutations by at least one caller were further filtered by comparing them with 1000 Genomes (internationalgenome.org), ExAC (exac.broadinstitute.org), ESP6500 (evs.gs.washington.edu) and ClinSeq (https://www.ncbi.nlm.nih.gov/projects/gap/cgi-bin/study.cgi?study_id=phs000971.v1.p1) databases; variants with minor allele frequency (MAF) > 1% were removed from further consideration. Variants in known false-positive genes[25] were excluded from further consideration.

Somatic mutation verification and deep NF1 mutation detection by Ampliseq/IonTorrent. Multiplex PCR primers for somatic mutation verification were designed using the Ion Ampliseq Designer tool (v.3.0.1, Life Technologies). Multiplex PCR amplification, library preparation and sequencing on the Ion Proton sequencer (Life Technologies) were performed as per the manufacturer's instructions.

Copy-number variation (CNV) and loss of heterozygosity (LOH). Single nucleotide polymorphism (SNP) genotyping was performed using HumanOmniExomeExpress BeadChip kits (Illumina, #20004207) as per the manufacturer's instructions. "Allele-Specific Copy number Analysis of Tumors" (ASCAT, v.2.1) analysis was performed as previously described[26]. For samples ANF1-ANF7, SNP-array data was not available. To analyze somatic copy-number alterations in the *NF1* and *CDKN2A/B* loci in these samples, we used ExomeCNV (v.1.4)[27] with the WES data. A CNV meta-analysis using previously published data[10] was performed. Paired CNV and LOH analysis of tumor and matching normal DNA was performed by using Nexus v.6.1 software (BioDiscovery Inc.) as described previously[28]. Genomic Identification of Significant Targets in Cancer (GISTIC) (https://software.broadinstitute.org/software/cprg/?q=node/31) analysis was performed using GISTIC module in Nexus v.6.1 software.

Whole transcriptome RNA sequencing and analysis of the data. Total RNA isolation, library construction and sequencing on the Illumina platform was done as previously described[15]. Expression

data was analyzed with Gene Set Enrichment Analysis (GSEA), version 2 (The Broad Institute; software.broadinstitute.org/gsea) according to the developer's recommendations.

Immunohistochemical (IHC) staining of tumors. All IHC stains were done on formalin-fixed paraffin embedded 5-micron tissue sections mounted on charged microscopic slides.

Results

Clinical characteristics of patients and tumors. Clinical information for the tumors and NF1 patients is summarized in Table 1 and a recent publication[9]. The pathologic classification of the ANF was done prior to the development of the new proposed term, "atypical neurofibromatous neoplasms of uncertain biologic potential" (ANNUBP) [20]. Hematoxylin and eosin (H&E) preps of select atypical neurofibromas are shown in comparison to PN and MPNST in Supplementary Fig. S1. While normal nuclei and typical plexiform architecture could be observed in PN, multiple instances of nuclear atypia, increased cellularity and loss of neurofibroma organization are prominent in the ANFs. On the other hand, in the high grade MPNST, multiple mitotic figures and a high degree of cellularity are well distinguished.

NF1, CDKN2A/B and PRC2 mutational and copy-number status in ANFs and MPNSTs. Information for the analyses performed on the tumor samples is available in Supplementary Table S1. We first sought mutations or deletions in *NF1* and *CDKN2A/B* (Table 2). We identified 14/14 (100%) and 13/16 (81%) *NF1* germline and somatic mutations, respectively, in the 16 ANFs. We identified no point mutations or small indels in *CDKN2A* or *CDKN2B*; however, SNP-array and ExomeCNV analyses revealed hetero- or homozygous loss of the *CDKN2A/2B* locus (9p21.3) in 12/16 (75%) tumors. We sought, but did not find, damaging somatic variation in PRC2 genes (*EED*, *SUZ12*, *EZH1/2*, *RBBP4/7*, *AEBP2*, *JARID2*) or in *TP53*.

In MPNSTs, we found pathogenic *NF1* germline and somatic mutations/deletions in 4/4 (100%) samples. There was heterozygous or homozygous loss of the *CDKN2A/B* locus in 4/4 (100%) MPNST. Like ANFs, we did not identify point mutations or small indels at this locus. We identified a potentially

deleterious homozygous missense mutation in *EED* (but intact *SUZ12*) in MPNST4 and a frame-shifting homozygous indel in *SUZ12* in MPNST3-1. In MPNST2, no PRC2 genes were mutated; however, expression of *SUZ12*, as demonstrated by RNAseq analysis, was sharply reduced in this tumor, implying that in some cases epigenetic inactivation of PRC2 genes could be at play (Supplementary Fig. S2A). The RNAseq findings for *SUZ12* expression in the MPNSTs were confirmed by immunohistochemistry staining with anti-SUZ12 antibodies: we observed robust SUZ12 expression in MPNST4 and sharply reduced levels of the protein in MPNST2 (Supplementary Fig. S2B). Interestingly, in MPNST3, in which *SUZ12* carried a homozygous frameshifting indel and in which the *SUZ12* RNA expression was at ~50% of normal (Supplementary Fig. S2A), we observed substantial tumor heterogeneity, with distinct areas in the tumor biopsy exhibiting drastically varying levels of SUZ12 expression (Supplementary Fig. S2B). It appears that in some MPNST3 cells the mutant protein is still expressed, however it is likely that its function is affected by this truncating mutation.

We observed a particularly informative case of a 9-year-old NF1 patient with a PN involving the right inguinal area, pelvis, and thigh (Fig. 1). MRI evaluation at NCI revealed two DNL in the inguinal and the paraspinal areas. Core biopsies of the inguinal and paraspinal lesions were classified as an ANF and neurofibroma, respectively. The inguinal lesion was later resected and the paraspinal tumor was observed. Genetic analysis of the paraspinal (ANF14-1) and inguinal nodular lesions (ANF14-2) confirmed that they originated within the same PN since they shared the same second hit in *NF1*. However, ANF14-1 and ANF14-2 harbor distinct deletions of chromosome 9p, which includes *CDKN2A/B* (Supplementary Fig. S3). These observations suggest that ANF14-1 and ANF14-2 arose within the PN and that deletion of *CDKN2A/B* is a predominant driving event in this transformation.

Small-scale somatic mutations in ANF and MPNST exomes. We identified 13 somatic mutations in 13 genes in nine ANF (Supplementary Table S2A). Of the 13 mutated genes, one (*FOXP1*) belonged to the COSMIC census of cancer genes. One tumor (ANF8) harbored five mutations in five different genes,

three of which were predicted to be damaging. All mutations in ANFs were heterozygous, with a median VAF of 0.21 (range 0.18 - 0.34); *NF1* was the only recurrently-mutated gene.

In contrast to ANFs, we observed 70 somatic mutations in three MPNSTs, 34 of which were potentially deleterious (Supplementary Table S2B). Unlike ANF mutations, 19/70 mutations in MPNSTs were homozygous (including *EED* and *SUZ12*), and the median VAF was 0.51 (range 0.15 – 1.00). One gene, *KAT7,* was mutated twice in a single tumor (MPNST2), but both mutations were in *cis*. *NF1* and PRC2 genes (*EED* and *SUZ12* in MPNST4 and MPNST3, respectively) were the only genes found recurrently mutated in the MPNSTs.

Chromosomal landscape of ANF and MPNST as revealed by allele-specific copy number analysis of tumors (ASCAT) analysis. Next, we used ASCAT to determine allele-specific copy number in 10 ANF and 4 MPNST. Most ANF were diploid, except for a single tumor (ANF13), which was nearly tetraploid. The median value of the fraction of atypical cells containing CNV in the ANFs was 40.5% (range 22–100%) (Supplementary Fig. S4A). Two of the MPNSTs (MPNST1 and MPNST2) were polyploid (4.03 and 4.82, respectively), while MPNST3 and MPNST4 were nearly diploid (1.72 and 1.91). The median proportion of aberrant cells in the MPNSTs was 96% (range 91-99%) (Supplementary Fig. S4B).

CNV meta-analysis of the combined ANF set. Next, we characterized individual CNVs in the combined set of 26 ANFs using Nexus and GISTIC analyses (Fig. 2). In 17/26 ANFs (65%), the most frequently affected locus was in 9p21.3, which harbors *CDKN2A/B* (Fig. 2B and Supplementary Fig. S5A). Most deletions were heterozygous. One deletion in one sample (A2) was called homozygous by the Nexus software, and additional six samples (A7_ANF5, A9, A12, A14, A16 and ANF10) had probe median Log2R ratio values considerably lower than the rest of the samples with the deletion (< -0.7), suggesting that the *CDKN2A/B* deletion in these samples was homozygous as well, a finding masked by heterogeneity of the tumors. We found several other regions adjacent to the *CDKN2A/B* locus on 9p that were deleted in more than one-third of the samples, but most of these regions were part of the larger

deletion spanning *CDKN2A/B*, implying that the majority of genes within these CNVs might simply be passengers (Fig. 2B). We identified one exception: *SMARCA2* was heterozygously deleted in 42% samples. In ~12% of ANF (A11_ANF7, A12, ANF11-7), the deletion was clearly independent from *CDKN2A/B* locus loss (Fig. S2B), suggesting a causative role of SWI/SNF complex disruption in tumor progression.

Among all ANF, we identified 253 genes that were affected in at least 4/26 samples. Eleven out of these 253 genes, including *CDKN2A*, were cancer genes (Supplementary Table S3A-C). One of them, *FANCG*, is a DNA repair protein implicated in maintenance of chromosome architecture (www.uniprot.org); frequent deletion of this gene could increase genomic instability, a common feature in MPNST. Another gene, *PTPRD*, is a tumor suppressor and a negative regulator of *STAT3* oncogene[29]. A frequent loss of *PTPRD* or *FANCG* in ANF warrants further investigation. The role of other genes (e.g., *JAK2*, *PDCD1LG2*, *PSIP1*, *FCGR2B*) that are predominantly deleted in ANF but are known as oncogenes or fusion genes is more challenging to define: it appears these genes are more likely to be passengers (Supplementary Table S3B).

CNV meta-analysis of the combined MPNST set. We observed a highly-rearranged genomic architecture in the MPNSTs (Fig. 2; Supplementary Fig. S5B). Like the ANFs, the *CDKN2A/B* locus was one of the most frequently deleted loci (20/28 [71%]) (Fig. 2B). Moreover, we observed a homozygous deletion of this locus in 14/28 (50%) samples, which was the most frequently observed homozygous loss in these tumors (Fig. 2B).

Across all samples, there were 23,229 genes affected by gains or losses in the regions that overlapped in at least 4/28 samples; 700 were cancer genes (Supplementary Table S3D-F). Out of these 700 genes, we identified 178 oncogenes that were at increased copy-number state, and 144 tumor suppressor genes (TSG) that were hetero- or homozygously deleted in at least 4/28 of samples (Supplementary Table S3E, F). We observed copy-number gains in receptor-tyrosine kinase (RTK) genes

that control cellular circuitry including RAS-MAPK, PI3K-AKT, PLC-gamma-PKC and JAK-STAT pathways (*e.g. EGFR, ERBB2/3/4*); signal transduction kinases/phosphatases (*e.g. BRAF, AKT2/3*); G1-S phase transition genes (*e.g. CDK6, CCND1/3*); negative regulators of TP53 (*PPM1D, MDM2/4*) and telomerase reverse transcriptase (*TERT*) among others. We detected gains and amplifications in *MYC* in 71% of samples and the transcriptional activator of *MYC*, *TRRAP*, was gained in 46% of samples. In addition to *MYC*, we identified increased copy number of *KLF4* and *SOX2*, the genes involved in maintaining "stemness" and pluripotency. *EZH2*, the methyl-transferase subunit of PRC2, was found at elevated copy-number state in 50% of MPNST.

In addition to multiple gains in oncogenes, we observed a number of losses in tumor-suppressor genes (TSG), including DNA repair/recombination genes (*e.g. ATM, PALB2*); chromatin modification genes, including PRC2 *EED* and *SUZ12* and subunits of chromatin remodeling complex SWI/SNF (*ARID1A, PBRM1)*, and genes controlling pluripotency of stem cells (*ZFHX3, JAK1, BMPR1A, AXIN1, TCF3, TBX3*).

GISTIC analysis of ANF and MPNST. We identified statistically significant CNVs (FDR<0.25) in 26 ANF and 28 MPNST by GISTIC (Fig. 2A; Supplementary Table S3G). Frequent loss of the *CDKN2A/B* locus was confirmed in both types of tumors. In MPNST, we confirmed frequent gain of oncogenes *MDM2* and *PDGFRA* and frequent loss of PRC2 genes *EED* and *SUZ12.*

Significant increase in genomic instability in transition from ANF to MPNST. We compared the median number of CNVs, median CNV size, median number of bases in all CNV combined in a tumor and the affected portion of the genome in ANF and MPNST (Table 3). There was a ~7-fold increase in the median number of CNV, a ~4-fold increase of the median size of CNV and a 33-fold increase of the affected portion of the genome (expressed either as a number of bases or percent of the genome) in MPNST *versus* ANF. *P-values* for all comparisons were $<10^{-5}$ (Mann-Whitney test), indicating a

substantially and significantly increased level of genomic instability in the transition from pre-malignant to malignant state.

Analysis of genome-wide expression RNAseq data by GSEA. We analyzed differential expression in ANFs and MPNSTs *versus* normal tissues using GSEA. Significant gene-sets up-regulated in ANF related to the immune response, signal transduction and processes affected in various types of cancer. Down-regulated gene-sets in ANF were associated with oxidative phosphorylation and cellular respiration. Up-regulated gene-sets in MPNST were associated with cell cycle, DNA replication/repair and chromosomal organization, while down-regulated gene-sets often included genes that were under-expressed in tumors with activated KRAS (Supplementary Table S4). There was a minimal overlap between significant gene-sets in ANF and MPNST (data not shown).

Next, we identified up- and down-regulated genes in ANF and MPNST that contributed to the enrichment score by performing leading edge analysis (LEA). There were 2,075 and 3,711 up-regulated, and 396 and 1,738 down-regulated genes in ANF and MPNST, respectively. Overlapping analysis between ANF and MPNST revealed 787 up- and 127 down-regulated genes in common. Both overlaps were highly statistically significant by the hypergeometric test. There were 30 known cancer genes among the genes in these overlaps (Supplementary Table S5). *CCND1*, *CDK6*, *NRAS*, *MDM2* and *MET* were among the overexpressed genes, and *AXIN2* was among the downregulated genes.

Differential expression of genes frequently affected by CNV/mutations, genes identified by GSEA leading edge analysis and select biologically-relevant genes. To better understand the transition of expression profiles from normal tissues to a premalignant state in ANF, we have included RNAseq data for 23 primary Schwann cell cultures established from NF1-associated plexiform neurofibromas (PN) and enriched for *NF1*$^{-/-}$ cells. First, we compared expression of 12 genes, including *NF1*, *CDKN2A/B*, *SMARCA2*, *NRAS*, PRC2 genes, *CCND1*, *CDK6*, *MDM2*, *TP53* in PN, ANF, MPNST and normal tissues (Fig. 3). In addition, we explored differential expression of genes associated with these 12 genes through participation in protein complexes, *e.g.*, SWI/SNF and PRC1/2, or signaling pathways, *e.g.* cell-cycle and

TP53 (Supplementary Fig. S6). We observed highly statistically significant over-expression of *NRAS* (but not *K*- and *HRAS*) in all three types of tumors: PN, ANF and in MPNST. Cell-cycle inhibitors *CDKN2A* and *CDKN2B* were expressed at very low levels in normal tissues, as expected. Sharply increased expression of these two genes in PN is likely due to inactivation of *NF1* and subsequent activation of *RAS*, which in turn mediates oncogene-induced senescence (see Discussion). In ANF and MPNST, where frequent deletion of the *CDKN2A/B* locus was observed, expression of these genes was predictably lower than in PN, but still higher than in normal tissues. We confirmed these observations by performing IHC analysis of PN, ANF and MPNST using anti-p16-INK4A antibodies: one can observe a robust expression of CDKN2A in most plexiform neurofibromas and substantially lower levels of this protein in ANF and MPNST (Supplementary Fig. S7). However, we observed a wide spectrum of intensities of p16 staining in the tumors, thus p16-INK4A IHC should be used in combination with other clinical and molecular analyses. Expression of cyclins D1 and D2 (*CCND1*/2) and *CDK4/6*, which control G1/S transition, was significantly higher in all three types of tumors compared with normal tissues (Supplementary Fig. S6A). We observed elevated expression of *MDM2* in all types of tumors as well; however, expression of *TP53*, which is the target of *MDM2* suppression, was mainly unchanged in the tumors (Supplementary Fig. S6B). We found that expression of *SUZ12* and *EED* was not significantly affected in the tumors; however, *EZH2*, the catalytic subunit of PRC2, was highly overexpressed in MPNST. In contrast, in ANF, expression of *EZH2* was similar to the normal controls (Supplementary Fig. S6C). Expression of *SMARCA2* in ANF was essentially the same as in normal tissues (Fig.3, Supplementary Fig. S6E), despite the observation that the gene was heterozygously deleted in 42% of the tumors. However, examination of the samples, which were used for the expression analysis, has shown that only one out of five samples carried heterozygous deletion of *SMARCA2*. In addition, ANF are heterogeneous tumors with a substantial proportion of the non-tumor cells, which further challenges accurate estimation of gene expression in these tumors. A modest but statistically significant downregulation of *SMARCA2* in the PNs (Fig. 3) warrants further investigation.

Discussion

This report is the first to describe comprehensive multi-platform genomic analyses of NF1-associated atypical neurofibromas from multiple patients. We show that *NF1* and *CDKN2A/B* loss are the primary genetic drivers in the development of ANF. In ANF, we observed *SMARCA2* loss in 42% of samples; we did not observe mutation or copy-number changes in *TP53* or the PRC2 complex. The overall somatic mutation burden in the ANFs was low, and similar to that observed in PN[15]. However, unlike in PN, where chromosomal architecture is essentially normal[15], we detected frequent (69%) deletions in chromosome 9p, which included *CDKN2A/B*. Overall, we observed a relatively low level of genomic instability in ANF and a profound, significantly increased perturbation of chromosomal architecture in MPNST, resulting in frequent gains of 178 oncogenes and in frequent losses in 144 TSG. Gene expression analysis with RNASeq revealed upregulated *NRAS*, *MDM2*, *CCND1/2/3* and *CDK4/6* in both ANF and MPNST, but *CCNA/E/B*, *CDK2/1*, *EZH2* as well as the genes controlling mitosis were overexpressed in MPNST only. We provide a case report of two genomically distinct ANFs (both harboring 9p [*CDKN2A/B*] deletions) that arose as radiographically distinct nodular lesions from the same PN in a child with NF1.

Nielsen and colleagues[14] observed that benign neurofibromas expressed p16, whereas the MPNSTs were essentially p16-negative. They concluded that inactivation of *CDKN2A* is associated with malignant transformation of neurofibromas. The most comprehensive study of ANF to date found one highly recurrent (15/16) deletion of the *CDKN2A/B* locus[10]. A recent study has demonstrated a normal status of *CDKN2A/B* in PN, but a deletion of this locus in two ANF resected from the same patient, and, importantly, that a copy-number status of *CDKN2A/B* correlated with a degree of histological atypia in these ANF.[30] Consistent with the previous studies, we identified hetero- or homozygous deletion of the *CDKN2A/B* locus as the most frequent genetic aberration in ANF tumors and one of the most frequent in MPNST.

In addition to frequent loss of *CDKN2A/B*, we found deletion of *SMARCA2* in 42% of ANF; moreover, in at least three samples the *SMARCA2* deletion was clearly separate from the *CDKN2A/B* loss pointing to a possible causative role of SWI/SNF complex disruption in the tumors. *SMARCA2* is an integral part of the ATP-dependent chromatin remodeling and transcriptional activator complex SWI/SNF, which in many instances acts as an antagonist of PRC1 and PRC2 complexes[31]. Given that the *CDKN2A/B* locus is itself a target for PRC1/2 inactivation[32], heterozygous deletion of *SMARCA2* may lead to a partial inactivation of SWI/SNF complex, which in turn may lower activity of p16INK4a/b and p14ARF by establishing more repressive chromatin structure by PRC1/2 at this locus. It will be important to further investigate what role inactivation of *SMARCA2* and other SWI/SNF genes might play in clinical severity of ANF.

In a first, we conducted RNASeq on ANFs. We acknowledge that the number of samples in our study was modest. Consistent with clinical observations that demonstrated continuous growth of ANF[8,9,33], we detected elevated expression of *NRAS*, *CCND1/2/3* and *CDK4/6* in these tumors. We detected elevated levels of *CDKN2A/B* in ANF compared to normal tissues, however, this is consistent with findings that an activated RAS-MAPK pathway (which in PNs is caused by *NF1* inactivation) induces senescence by stimulating these cell cycle inhibitors[34]. The frequent deletions of the *CDKN2A/B* locus that we observed in ANF may aid in overcoming p16-, p15- and p14-mediated inhibition of the cell cycle in these tumors and, in turn, activate *MDM2*, which was also one of the genes with frequent gains in the MPNST and overexpressed in both types of tumors. Interestingly, in a recent study [35] it was demonstrated that *MDM2* directly binds to *EZH2* and modifies methylation of histones, thus promoting stemness and enabling cancer cell survival independently of p53. In light of these observations, inhibition of *MDM2* and/or *EZH2* in MPNST might be an appealing therapeutic strategy.

At present, the diagnosis of ANF is difficult and primarily is based on pathological examination of the tumors. A new term, "atypical neurofibromatous neoplasms of uncertain biologic potential (ANNUBP)," and diagnostic criteria have been recently proposed[20]. In this study, we evaluated two

distinct ANFs (ANF14-1 and ANF14-2) from an NF1 patient and arising from the same PN. Although clinically both lesions were worrisome, the pathology examination classified only one tumor as an ANF, while deeming the other as benign neurofibroma. Subsequent genomic analysis of the tumors revealed that both lesions had concerning *CDKN2A/B* locus deletion. Careful re-examination of the tumors by the pathologist left the diagnoses unchanged; however, based on clinical and genetic evidence, we believe that both tumors should be treated as ANF. This example underscores importance of genetic information in clinical decision making and illustrates that PN-ANF transformation could be relatively frequent, at least in some patients.

In conclusion, in our data, in addition to PN-related *NF1* inactivation, transition from benign PN to pre-malignant ANF frequently proceeds through inactivation of *CDKN2A/B*. *CDKN2A/B* appears to be the primary driver of this transition, but perhaps other genetic events (*e.g.*, deletion of *SMARCA2*) are also involved. Upon further transformation to the malignant state the level of genomic instability rises dramatically, accelerating complete loss of function of key gatekeepers via LOH (e.g., *EED* and *SUZ12*) and by affecting copy-number of multiple oncogenes and TSG.

The content of this publication does not necessarily reflect the views or policies of the Department of Health and Human Services, nor does mention of trade names, commercial products or organizations imply endorsement by the U.S. Government.

References

1 Uusitalo, E. *et al.* Incidence and mortality of neurofibromatosis: a total population study in Finland. *J Invest Dermatol* **135**, 904-906, doi:10.1038/jid.2014.465 (2015).

2 Friedman, J. M. in *GeneReviews(R)* (eds R. A. Pagon *et al.*) (University of Washington, Seattle University of Washington, Seattle. All rights reserved., 1993).

3 Evans, D. G. *et al.* Mortality in neurofibromatosis 1: in North West England: an assessment of actuarial survival in a region of the UK since 1989. *Eur J Hum Genet* **19**, 1187-1191, doi:10.1038/ejhg.2011.113 (2011).

4 Uusitalo, E. *et al.* Distinctive Cancer Associations in Patients With Neurofibromatosis Type 1. *J Clin Oncol* **34**, 1978-1986, doi:10.1200/JCO.2015.65.3576 (2016).

5 Evans, D. G. *et al.* Malignant peripheral nerve sheath tumours in neurofibromatosis 1. *Journal of medical genetics* **39**, 311-314 (2002).

6 Mautner, V. F. *et al.* Assessment of benign tumor burden by whole-body MRI in patients with neurofibromatosis 1. *Neuro Oncol* **10**, 593-598, doi:10.1215/15228517-2008-011 (2008).

7 Kim, A. *et al.* Malignant Peripheral Nerve Sheath Tumors State of the Science: Leveraging Clinical and Biological Insights into Effective Therapies. *Sarcoma* **2017**, 7429697, doi:10.1155/2017/7429697 (2017).

8 Meany, H. *et al.* 18-fluorodeoxyglucose-positron emission tomography (FDG-PET) evaluation of nodular lesions in patients with Neurofibromatosis type 1 and plexiform neurofibromas (PN) or malignant peripheral nerve sheath tumors (MPNST). *Pediatr Blood Cancer* **60**, 59-64, doi:10.1002/pbc.24212 (2013).

9 Higham, C. S. *et al.* The Characteristics of 76 Atypical Neurofibromas as Precursors to Neurofibromatosis 1 Associated Malignant Peripheral nerve Sheath Tumors. *Neuro Oncol*, doi:10.1093/neuonc/noy013 (2018).

10 Beert, E. *et al.* Atypical neurofibromas in neurofibromatosis type 1 are premalignant tumors. *Genes Chromosomes Cancer* **50**, 1021-1032, doi:10.1002/gcc.20921 (2011).

11 Berner, J. M. *et al.* Chromosome band 9p21 is frequently altered in malignant peripheral nerve sheath tumors: studies of CDKN2A and other genes of the pRB pathway. *Genes Chromosomes Cancer* **26**, 151-160 (1999).

12 Kourea, H. P., Orlow, I., Scheithauer, B. W., Cordon-Cardo, C. & Woodruff, J. M. Deletions of the INK4A gene occur in malignant peripheral nerve sheath tumors but not in neurofibromas. *The American journal of pathology* **155**, 1855-1860, doi:10.1016/s0002-9440(10)65504-6 (1999).

13 Mantripragada, K. K. *et al.* High-resolution DNA copy number profiling of malignant peripheral nerve sheath tumors using targeted microarray-based comparative genomic hybridization. *Clin Cancer Res* **14**, 1015-1024, doi:10.1158/1078-0432.CCR-07-1305 (2008).

14 Nielsen, G. P. *et al.* Malignant transformation of neurofibromas in neurofibromatosis 1 is associated with CDKN2A/p16 inactivation. *The American journal of pathology* **155**, 1879-1884, doi:10.1016/s0002-9440(10)65507-1 (1999).

15 Pemov, A. *et al.* The primacy of NF1 loss as the driver of tumorigenesis in neurofibromatosis type 1-associated plexiform neurofibromas. *Oncogene* **36**, 3168-3177, doi:10.1038/onc.2016.464 (2017).

16 Lee, W. *et al.* PRC2 is recurrently inactivated through EED or SUZ12 loss in malignant peripheral nerve sheath tumors. *Nat Genet* **46**, 1227-1232, doi:10.1038/ng.3095 (2014).

17 Zhang, M. *et al.* Somatic mutations of SUZ12 in malignant peripheral nerve sheath tumors. *Nat Genet* **46**, 1170-1172, doi:10.1038/ng.3116 (2014).

18 De Raedt, T. *et al.* PRC2 loss amplifies Ras-driven transcription and confers sensitivity to BRD4-based therapies. *Nature* **514**, 247-251, doi:10.1038/nature13561 (2014).

19 Reilly, K. M. *et al.* Neurofibromatosis Type 1-Associated MPNST State of the Science: Outlining a Research Agenda for the Future. *Journal of the National Cancer Institute* **109**, doi:10.1093/jnci/djx124 (2017).

20 Miettinen, M. M. *et al.* Histopathologic evaluation of atypical neurofibromatous tumors and their transformation into malignant peripheral nerve sheath tumor in patients with neurofibromatosis 1-a consensus overview. *Hum Pathol* **67**, 1-10, doi:10.1016/j.humpath.2017.05.010 (2017).

21 Cibulskis, K. *et al.* Sensitive detection of somatic point mutations in impure and heterogeneous cancer samples. *Nat Biotechnol* **31**, 213-219, doi:10.1038/nbt.2514 (2013).

22 Larson, D. E. *et al.* SomaticSniper: identification of somatic point mutations in whole genome sequencing data. *Bioinformatics* **28**, 311-317, doi:10.1093/bioinformatics/btr665 (2012).

23 Hansen, N. F., Gartner, J. J., Mei, L., Samuels, Y. & Mullikin, J. C. Shimmer: detection of genetic alterations in tumors using next-generation sequence data. *Bioinformatics* **29**, 1498-1503, doi:10.1093/bioinformatics/btt183 (2013).

24 Saunders, C. T. *et al.* Strelka: accurate somatic small-variant calling from sequenced tumor-normal sample pairs. *Bioinformatics* **28**, 1811-1817, doi:10.1093/bioinformatics/bts271 (2012).

25 Fuentes Fajardo, K. V. *et al.* Detecting false-positive signals in exome sequencing. *Hum Mutat* **33**, 609-613, doi:10.1002/humu.22033 (2012).

26 Van Loo, P. *et al.* Analyzing cancer samples with SNP arrays. *Methods Mol Biol* **802**, 57-72, doi:10.1007/978-1-61779-400-1_4 (2012).

27 Sathirapongsasuti, J. F. *et al.* Exome sequencing-based copy-number variation and loss of heterozygosity detection: ExomeCNV. *Bioinformatics* **27**, 2648-2654, doi:10.1093/bioinformatics/btr462 (2011).

28 Dewan, R. *et al.* Evidence of polyclonality in neurofibromatosis type 2-associated multilobulated vestibular schwannomas. *Neuro Oncol* **17**, 566-573, doi:10.1093/neuonc/nou317 (2015).

29 Kim, M., Morales, L. D., Jang, I. S., Cho, Y. Y. & Kim, D. J. Protein Tyrosine Phosphatases as Potential Regulators of STAT3 Signaling. *International journal of molecular sciences* **19**, doi:10.3390/ijms19092708 (2018).

30 Carrio, M. *et al.* Analysis of intratumor heterogeneity in Neurofibromatosis type 1 plexiform neurofibromas and neurofibromas with atypical features: Correlating histological and genomic findings. *Hum Mutat* **39**, 1112-1125, doi:10.1002/humu.23552 (2018).

31 Kadoch, C., Copeland, R. A. & Keilhack, H. PRC2 and SWI/SNF Chromatin Remodeling Complexes in Health and Disease. *Biochemistry* **55**, 1600-1614, doi:10.1021/acs.biochem.5b01191 (2016).

32 Gil, J. & Peters, G. Regulation of the INK4b-ARF-INK4a tumour suppressor locus: all for one or one for all. *Nat Rev Mol Cell Biol* **7**, 667-677, doi:10.1038/nrm1987 (2006).

33 Ferner, R. E. [18F]2-fluoro-2-deoxy-D-glucose positron emission tomography (FDG PET) as a diagnostic tool for neurofibromatosis 1 (NF1) associated malignant peripheral nerve sheath tumours (MPNSTs): a long-term clinical study. (2008).

34 DeNicola, G. M. & Tuveson, D. A. RAS in cellular transformation and senescence. *European journal of cancer (Oxford, England : 1990)* **45 Suppl 1**, 211-216, doi:10.1016/s0959-8049(09)70036-x (2009).

35 Wienken, M. *et al.* MDM2 Associates with Polycomb Repressor Complex 2 and Enhances Stemness-Promoting Chromatin Modifications Independent of p53. *Mol Cell* **61**, 68-83, doi:10.1016/j.molcel.2015.12.008 (2016).

Figure Legends

Fig. 1 MRI and FDG-PET evaluation of two distinct nodular lesions within a single large plexiform neurofibroma (PN). **A** and **B** A 9-year old boy with NF1 and newly diagnosed plexiform neurofibroma involving the right retroperitoneum, pelvis, and thigh. MRI evaluation at the NCI revealed two distinct nodular lesions, one in the right inguinal area (**A**; sample ANF14-2), and one in the right paraspinal area (**B**; sample ANF14-1). **C, D** and **E** Volumetric MRI analysis demonstrated faster growth rates for the nodular lesions (black contour) compared with the plexiform neurofibroma (green contour). **F** and **G** FDG-PET demonstrated FDG-avidity of the nodular lesions with minimal uptake in the surrounding plexiform neurofibroma (**F** and **G**, inguinal and paraspinal lesions, respectively). Core biopsy of the inguinal lesion showed atypical neurofibroma; core biopsy of the paraspinal lesion showed neurofibroma. The inguinal lesion was resected, and pathology confirmed atypical neurofibroma. Follow-up with MRI continues to demonstrate more rapid growth of the remaining paraspinal lesion compared with the plexiform neurofibroma (**C** and **D**).

Fig. 2 Copy-number variation in ANF and MPNST. **A** GISTIC analysis of 26 ANF (upper panel) and 28 MPNST (lower panel). Gains and losses are shown in blue and red, respectively. Statistically significant CNVs (FDR<0.25) are denoted with grey vertical bars. Chromosome numbers are shown on top of each panel. **B** Copy-number variation in chromosome 9p in 26 ANF (left panel) and 28 MPNST (right panel). Gains and losses are shown in blue and red, respectively. Homozygous losses are shown in dark red and thick bars. Vertical rectangles in the center denote minimally overlapped regions in ANF and MPNST that both include the *CDKN2A* and *CDKN2B* genes. Left vertical rectangle in the ANF panel denotes *SMARCA2*. Arrows show samples (A11_ANF7, A12, ANF11-7), in which deletion of *SMARCA2* is clearly independent from *CDKN2A/B.*

Fig. 3 Expression of genes frequently affected by CNV/mutations, genes identified by GSEA leading edge analysis and select biologically relevant genes in normal tissues (n=39), PN (n=23), ANF (n=5) and MPNST (n=5) as determined by RNAseq analysis. Expression values are shown in Fragments Per

Kilobase per Million reads, Log2 transformed, (Log2(FPKM)) units. Blue, red, grey and orange bars correspond to normal tissues, PN, ANF and MPNST, respectively. Asterisks indicate statistically significant difference (by two-tail t-tests) between normal and PN, ANF or MPNST expression values at $p < 0.0001$.

Tumor sample ID	**Tumor ID in Higham et al., 2018**	**Tumor type**	**Age at diagnosis (years)**	**Sex**	**Inheritance**	**Family history of MPNST**	**Personal history of MPNST**	**Location**	**Reason for biopsy/ resection**	**Additional concerning lesions**	**Isolated or within plexiform**
A15_ANF1	BEL-13-1	ANF	26.9	M	Unknown	NA	No	Neck	G	Yes	Isolated
ANF2	BEL-17	ANF	34.4	F	Sporadic	No	Yes	Neck	P, G	No	Isolated
A13_ANF3	BEL-11	ANF	58.8	F	Unknown	NA	No	Neck	P, G, E	No	Isolated
A4_ANF4	BEL-4	ANF	28.3	M	Familial-Maternal	NA	Yes	Abdomen/Pelvis	E	No	Unknown
A7_ANF5	N/A	ANF	18.8	F	Sporadic	No	No	Chest	G, E	No	Within PN
ANF6	BEL-16	ANF	32.7	F	Unknown	NA	No	Lower extremity	P	No	Within PN
A11_ANF7	N/A	ANF	26.7	F	Familial-Maternal	No	Yes	Neck	P	Yes	Unknown
ANF8	BEL-14	ANF	28.3	F	Familial-Matern	NA	No	Chest	P, G	No	Unknown

					al						
ANF9	N/A	ANF	26.4	M	Familial-Maternal	NA	No	Lower extremity	P	No	Unknown
ANF10	BEL-18	ANF	31.8	F	Unknown	NA	No	Chest	G, E	No	Isolated
ANF11-1[a]	NCI-14-3	ANF	28.3	M	Familial-Paternal	No	No	Abdomen/Pelvis	G, E	Yes	Within PN
ANF11-2[a]	NCI-14-3	ANF	28.3	M	Familial-Paternal	No	No	Abdomen/Pelvis	G, E	Yes	Within PN
ANF11-6	NCI-14-4	ANF	30.4	M	Familial-Paternal	No	No	Lower extremity	E	Yes	Isolated
ANF11-7	NCI-14-1	ANF	25.4	M	Familial-Paternal	No	No	Abdomen/Pelvis	G, E	Yes	Within PN
ANF13-1	NCI-15	ANF	26	F	Familial-Paternal	Yes	Yes	Lower extremity	G, E	Yes	Isolated
ANF14-1[b]	N/A	NF/ANF[&]	9.4	M	Sporadic	No	No	Abdomen/Pelvis	G, E	No	Within PN
ANF14-2[b]	NCI-2	ANF	9.4	M	Sporadic	No	No	Abdomen/Pelvis	G, E	No	Within PN
ANF15	NCI-3	ANF	13.7	M	Familial-Maternal	Yes	No	Lower extremity	G, E	Yes	Isolated

MPNST T1	N/A	MPNST	17.1	M	Familial-Maternal	No	Yes[d]	Abdomen/Pelvis	P, G, E	No	Within PN
MPNST T2	N/A	MPNST	47	M	Sporadic	No	Yes	Upper extremity	P, G	No	Within PN
MPNST T3-1[c]	N/A	MPNST	23.6	M	Sporadic	No	Yes[d]	Abdomen/Pelvis	P, G, E	Yes	Within PN
MPNST T3-2[c]	N/A	MPNST	23.6	M	Sporadic	No	Yes[d]	Abdomen/Pelvis	P, G, E	Yes	Within PN
MPNST T4	N/A	MPNST	28	M	Sporadic	No	Yes	Lower extremity	P, G	No	Within PN
MPNST T5	N/A	MPNST	39	M	Sporadic	No	Yes	Brain metastasis[e]	Neurological symptoms	No	Brain metastasis

Table 1. Clinical information for patients and tumors. Abbreviations: NA = Not Available, N/A = Not Applicable; P = pain associated with tumor; G = tumor growth; E = elevated SUV on FDG-PET; F = female; M = male; SUV = Standardized Uptake Value; FDG-PET = Fluorodeoxyglucose-Positron Emission Tomography; MPNST = Malignant Peripheral Nerve Sheath Tumor; ANF = Atypical Neurofibroma. Superscripts: a) - fragments of a larger tumor; b) - two distinct nodular lesions within the same plexiform neurofibroma; c) - fragments of a larger tumor; d) - lesions included in this study; e) - primary MPNST in a leg; &) - tumor ANF14-1 was initially classified as neurofibroma (NF) by a pathologist, however, based on clinical (fast growth and elevated SUV on FDG-PET scan) and genetic (deletion of the *CDKN2A/B* locus) evaluations in this study, this tumor was reclassified as ANF. IDs for ANF investigated in Higham et al., 2018 (*Neuro-Oncology, Vol. 20, pp. 818-825*) are shown in the second column.

Sample ID	*NF1*, germline	*NF1*, somatic	*CDKN2A/2B*	PRC2 genes
A15_ANF1	Frameshift, p.M991fs	Gains with multiple breakpoints*	***Not detected***	***Not detected***
ANF2[a]	Missense, p.A706F	***Not detected***	***Not detected***	***Not detected***
A13_ANF3	Splicing, c.3113+1G>A	Frameshift, p.E2645fs	Het loss	***Not detected***
A4_ANF4	Type I microdeletion	Nonsense, p.Q1822X	***Not detected***	***Not detected***
A7_ANF5	Frameshift, c.595_597TT	Large deletion	Homozygous loss	***Not detected***
ANF6[a]	Exons 2-28 deletion	***Not detected***	***Not detected***	***Not detected***
ANF7	Splicing, c.3113+1G>A	Frameshift, c.7901_7905T	Homozygous loss	***Not detected***
ANF8	Missense, p.L2338P	Large deletion*	Het loss	***Not detected***
ANF9	Missense, p.Y575C	Missense, p.C845Y	Partial gain, with a breakpoint in *CDKN2A*	***Not detected***
ANF10	Splicing, c.1261-1G>A	Frameshift, c.668_670GG	Homozygous loss	***Not detected***
ANF11-1	Frameshift, p.1603_1604del	Copy-neutral LOH	Het loss	***Not detected***
ANF11-2	Same as in ANF11-1	Copy-neutral LOH	Het loss	***Not detected***
ANF13	Nonsense, p.R416X	***Not detected***	Het loss	***Not detected***
ANF14-1	Splicing, c.288+2T>G	Frameshift, p.I1402fs	Het loss	***Not detected***
ANF14-2	Same as in ANF14-1	Same as in ANF14-1	Het loss	***Not detected***
ANF15	Frameshift, c.6850_6855AC	Frameshift, c.7990_7991A	Partial gain, with a breakpoint in *CDKN2A*	***Not detected***
MPNST1	Nonsense, p.R440X	Frameshift, p.L995fs	Homozygous loss	Not available

MPNST2	Nonsense, p.R1276X	Copy-neutral LOH	Homozygous loss *CDKN2A*, Het loss *CDKN2B*	Not detected, but *SUZ12* expression is sharply decreased
MPNST3-1	Frameshift, c.6212_6213A	Large deletion	Het loss	*SUZ12*, p.T412fs, homozygous
MPNST4	Frameshift, p.A1228fs	Copy-neutral LOH	Homozygous loss	*EED*, p.S241R, homozygous
Detection rate in ANF	**100% (14/14)**	**81% (13/16)**	**75% (12/16)**	**0% (0/16)**
Detection rate in MPNST	**100% (4/4)**	**100% (4/4)**	**100% (4/4)**	**67% (2/3)**

Table 2. Mutation and copy-number variation in *NF1, CDKN2A/B* and PRC2 genes in ANF and MPNST. Mutations are highlighted by a color fill. Abbreviations: Het = Heterozygous; LOH = Loss of Heterozygosity. Superscripts: a) - only ExomeCNV (v.1.4) analysis of the WES data for the *NF1* and *CDKN2A/B* loci was performed; b) - copy-number changes detected in WES data only.

Figure 1

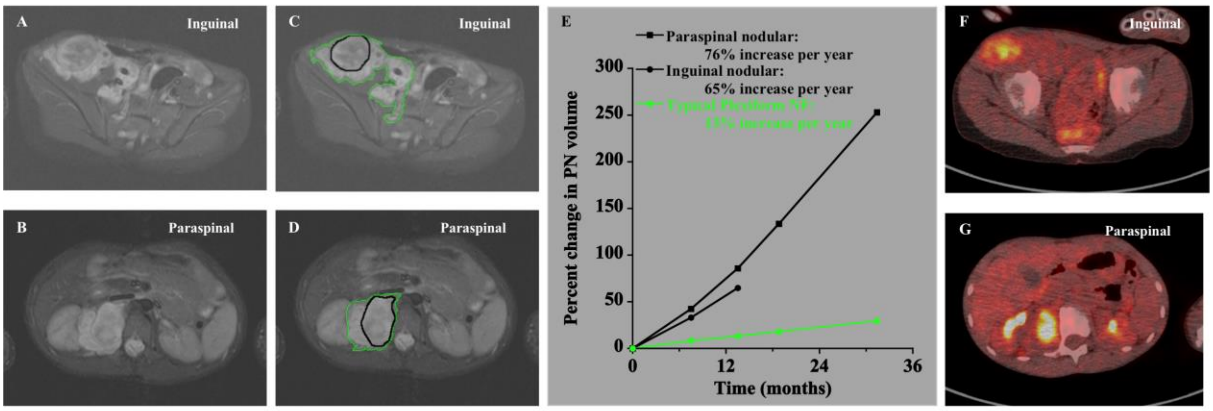

Fig. 1

Figure 2

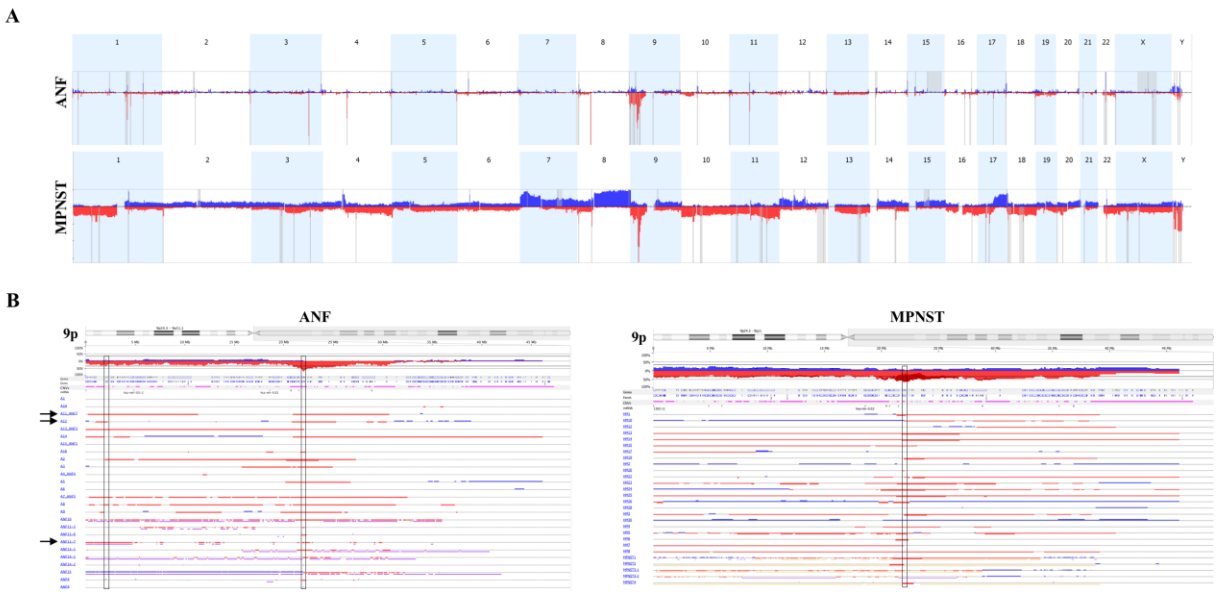

Fig. 2

Figure 2A

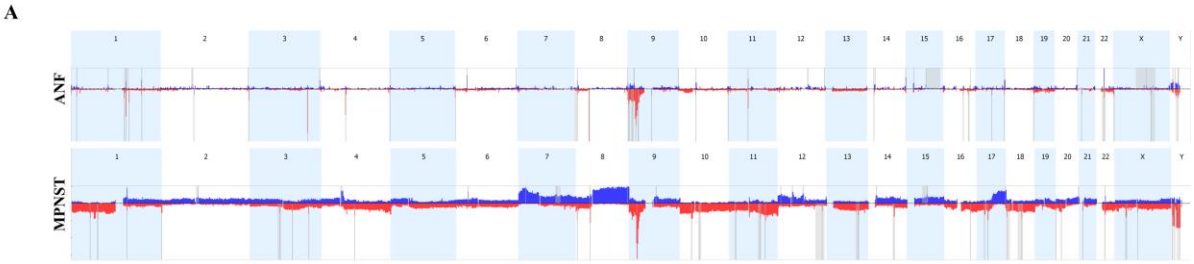

Figure 2B

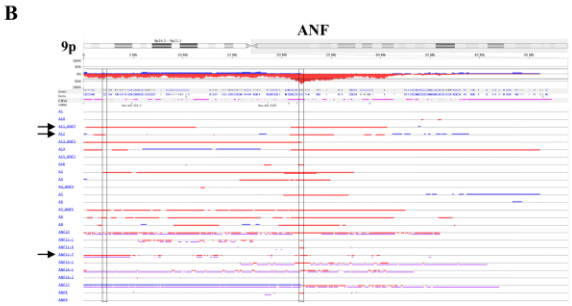

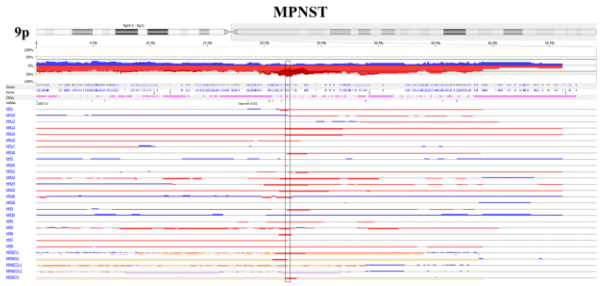

Figure 3